Since January 2020 Elsevier has created a COVID-19 resource centre with free information in English and Mandarin on the novel coronavirus COVID-19. The COVID-19 resource centre is hosted on Elsevier Connect, the company's public news and information website.

Biochemical and Biophysical Research Communications 477 (2016) 383–387

Contents lists available at ScienceDirect

Biochemical and Biophysical Research Communications

journal homepage: www.elsevier.com/locate/ybbrc

Crystal structure of an acetyl esterase complexed with acetate ion provides insights into the catalytic mechanism

Keiko Uechi [a], Saori Kamachi [a], Hironaga Akita [a], Shouhei Mine [b], Masahiro Watanabe [a, *]

[a] Research Institute for Sustainable Chemistry, National Institute of Advanced Industrial Science and Technology (AIST), 3-11-32 Kagamiyama, Higashi-Hiroshima, Hiroshima 739-0046, Japan

[b] Biomedical Research Institute (BMD), National Institute of Advanced Industrial Science and Technology (AIST), 1-8-31 Midorigaoka, Ikeda, Osaka, 563-8577, Japan

ARTICLE INFO

Article history:
Received 2 June 2016
Accepted 18 June 2016
Available online 18 June 2016

Keywords:
Acetyl esterase
Carbohydrate esterase family 3
Talaromyces cellulolyticus
SGNH-hydrolase
Catalytic triad
Oxyanion hole

ABSTRACT

We previously reported the crystal structure of an acetyl esterase (TcAE206) belonging to carbohydrate esterase family 3 from *Talaromyces cellulolyticus*. In this study, we solved the crystal structure of an S10A mutant of TcAE206 complexed with an acetate ion. The acetate ion was stabilized by three hydrogen bonds in the oxyanion hole instead of a water molecule as in the structure of wild-type TcAE206. Furthermore, the catalytic triad residue His182 moved 0.8 Å toward the acetate ion upon substrate entering the active site, suggesting that this movement is necessary for completion of the catalytic reaction.

1. Introduction

The lignocellulose component of the plant cell wall is composed of cellulose, hemicellulose, and lignin [1,2]. Microbial degradation of lignocellulosic biomass in animal feed and food production, and softwood pulp bleaching in paper production is of increasing industrial significance [3–6]. Hemicelluloses are either highly or partially acetylated, which strongly inhibits degradation by polysaccharide-hydrolyzing enzymes [6]. However, the activity of major hemicellulose-hydrolyzing enzymes such as xylanases and mannanases can be enhanced by the enzymes acetylxylan esterase and acetyl esterase, which remove acetyl groups from hemicellulose [7,8]. Carbohydrate esterases (CE), which includes acetylxylan and acetyl esterase, are categorized into 16 families (CE1–16) within the CAZy database (http://www.cazy.org/Carbohydrate-Esterases.html) [9]. With the exception of CE4, most CE family enzymes contain an α/β-hydrolase fold and function as serine esterases via a catalytic triad [10–13].

The crystal structures of bacterial CE3 enzymes, which are acetylxylan esterases, have been reported for *Clostridium thermocellum* (CtCes3-1; PDB code 2vpt) [14] and *Sinorhizobium meliloti* (Sm23; PDB code 4tx1) [15]. We recently reported the crystal structure of a fungal CE3 acetyl esterase with a catalytic domain from *Talaromyces cellulolyticus* (TcAE206; PDB code 5b5s, previous PDB code 3x0h) [16]. Even though the structure of TcAE206 is similar to that of other CE3 enzymes, its substrate specificity differs considerably. TcAE206 exhibits enzymatic activity against acetylated oligosaccharides but not acetylated xylans [16]. In contrast, CtCes3-1 shows enzymatic activity against acetylated xylans and oligosaccharides [14] The substrate specificity of Sm23 was omitted from this comparison because acetylated xylans and oligosaccharides were not used as substrates [15]. The manner in which the acetylated carbohydrate moiety binds has yet to be fully elucidated, however. Here, we report for the first time the substrate/product complex structure of a CE3 family enzyme and discuss the substrate-induced conformational change in the generally basic residue His182.

Abbreviation: TcAE206, the catalytic domain of acetylesterase from *Talaromyces cellulolyticus*; S10A, mutant of TcAE206 substituted serine 10 with alanine; CE, carbohydrate esterase; CtCes3-1, acetylxylan esterase from *Clostridium thermocellum*; Sm23, acetylxylan esterase from *Sinorhizobium meliloti*; RMSD, root mean square deviation.

* Corresponding author. Tel.: +81 82 420 8285; fax: +81 82 423 7820.
E-mail address: masa-watanabe@aist.go.jp (M. Watanabe).

http://dx.doi.org/10.1016/j.bbrc.2016.06.093
0006-291X/

2. Materials and methods

2.1. Protein expression and purification

An expression vector (pS10A) for substituting TcAE206 Ser10 with an Ala residue was constructed by site-directed mutagenesis as described previously [16]. *Escherichia coli* BL21 (DE3) harboring pS10A was cultivated and induced as described previously [16]. The cells were then harvested by centrifugation, dissolved in 20 mM Tris-HCl (pH 8.0) containing 50 mM NaCl, and stored at −80 °C. The cells were lysed by three cycles of freezing-thawing, and the resulting lysate was centrifuged (35,870 × g for 20 min at 4 °C); the resulting supernatant including mutant of TcAE206 (S10A) was loaded onto a HiTrap Q column (GE Healthcare, Buckinghamshire, UK) equilibrated with 20 mM Tris-HCl (pH 8.0) and eluted using a linear gradient of 0.0–1.0 M NaCl in the same buffer. The collected active fractions were saturated with 1.0 M $(NH_4)_2SO_4$ and then loaded onto a HiTrap PHE column (GE Healthcare) previously equilibrated with the same buffer containing 1.0 M $(NH_4)_2SO_4$. The enzyme was eluted with a linear 1.0–0.0 M $(NH_4)_2SO_4$ gradient. The active fractions were pooled, concentrated, and loaded onto a Superdex 200 pg gel filtration column (GE Healthcare) equilibrated with 20 mM Tris-HCl (pH 8.0) containing 50 mM NaCl. The purity of the target protein was confirmed by SDS-PAGE. The protein concentration was determined by measuring the absorption at 280 nm. The protein was then concentrated to 12 mg mL^{-1} in 20 mM Tris-HCl buffer (pH 8.0).

2.2. Crystallization and X-ray diffraction analysis

The initial crystallization screening of S10A was performed using Crystal Screen HT (Hampton Research) at 20 °C by the sitting-drop vapor diffusion method, in which a 0.5-μL volume of protein solution was mixed with an equal volume of reservoir solution. Small crystals were grown for 1 day in reagent No. G3, 0.1 M 2-morpholinoethanesulfonic acid (MES) buffer (pH 6.5), 25% (v/v) polyethylene glycol monomethyl ester (PEGME) 550, and 10 mM $ZnSO_4$. The crystallization conditions were optimized using the hanging-drop vapor diffusion method, in which a 2.0-μL volume of protein solution was mixed with an equal volume of reservoir solution. S10A, with 10 mM D-glucose pentaacetate (Sigma-Aldrich, St. Louis, MO, USA), was crystallized in 0.1 M MES buffer (pH 6.5), 15–20% (v/v) PEGME 550, and 10 mM $ZnSO_4$ for 3 days at 20 °C. The resulting crystals were then soaked in reservoir solution containing 25% (v/v) polyethylene glycol 400 as a cryoprotectant. X-ray diffraction data for the S10A–acetate ion crystals were collected at the beamline BL44XU at SPring-8 (Hyogo, Japan) using 0.9-Å wavelength radiation. A total 180° of data were collected using a Rayonix MX300-HE CCD detector. All data were processed to 1.40-Å resolution using HKL2000 (DENZO and SCALEPACK) [17].

2.3. Phasing, refinement, and structural analysis

General data handling was carried out using the CCP4 package [18]. The initial model of the S10A mutant complexed with acetate ion was determined by molecular replacement using PHASER [19] with a search model of TcAE206 (PDB code 5b5s). The final model was built using COOT [20], and refinements were carried out using REFMAC5 [21]. Water molecules were added using COOT, and model geometry was analyzed using RAMPAGE [22]. Molecular graphics figures were created using PyMOL (http://pymol.sourceforge.net/) [23].

3. Results and discussion

3.1. Overall structure of TcAE206_S10A complexed with acetate ion

The complex structure of S10A–acetate ion was solved at 1.4-Å resolution. The prepared crystals belonged to space group $P3_221$, with unit cell a = b = 64.6 Å and c = 89.6 Å. The asymmetric unit consisted of one molecule with a solvent content of 49.4%, which corresponded to a Matthews coefficient of 2.43 $Å^3$ Da^{-1} [24]. After refinement, R_{work} was estimated at 12.2%, and R_{free} was estimated at 17.4%. Data collection and refinement statistics are shown in Table 1. The overall structure of S10A was constructed from Met1 to Ser207, with an acetate ion, solvent molecules, and metal ions. There was no major difference in overall structure between S10A and wild-type TcAE206 [16], with the root mean square deviation (RMSD) of 0.4 Å over 207 Cα atoms. Briefly, the structure of S10A formed an α/β-hydrolase fold and canonical SGNH-hydrolase superfamily fold comprising five central parallel β-strands and flanked by six α-helices, with a classic serine esterase catalytic triad (Ser-Asp-His).

The catalytic domain structure of TcAE206 is similar to the structures of CtCes3-1 (Z-score of 25.5 and RMSD of 2.0 Å over 192 Cα atoms) and Sm23 (Z-score of 19.8 and RMSD of 1.9 Å over 168 Cα atoms) [14–16]. In addition, the major residues constituting the catalytic triad (Ser10, Asp180, and His182) and oxyanion hole (Ser10, Gly62, and Asn92) in the active site of TcAE206 are completely conserved in CtCes3-1 (Ser44, Asp205, His208, Gly95, and Asn124) and Sm23 (Ser10, Asp187, His190, Gly50, and Asn90) (Supplementary Fig. S1). The coordinates and structural factors for TcAE206_S10A were deposited in the Protein Data Bank under the accession code 5B5L.

Table 1
Data collection and refinement statistics.

Data collection	
Wavelength (Å)	0.9
Space group	$P3_221$
Unit cell (a, b, c (Å))	64.6, 64.6, 89.7
(α, β, γ (°))	90, 90, 120
Resolution range (Å)	50.0–1.40 (1.42–1.40)[a]
Total No. of reflections	245,260
No. of unique reflections	42,027
Redundancy	5.8 (3.5)[a]
Completeness (%)	97.4 (94.2)[a]
R_{merge} (%)[b]	8.3 (37.3)[a]
$< I/\sigma(I) >$	43.8 (4.4)[a]
Refinement	
Resolution range (Å)	30.0–1.40
R_{work} (%)[c]/R_{free} (%)[d]	12.1/17.4
No. of protein atoms	1578
No. of ligands	10
No. of water molecules	202
RMSD	
Bond lengths (Å)	0.034
Bond angles (°)	2.3
Average *B* factor (Å^2)	17.1
Ramachandran statistics (%)	
Favored region	95.6
Allowed region	4.4
PDB accession number	5B5L

[a] Outer shell (1.42–1.40 Å).
[b] $R_{merge} = \sum_{hkl}\sum_i|I_i(hkl)-\langle I(hkl)\rangle|/\sum_{hkl}\sum_i Ii(hkl)$, where I_i(hkl) is the scaled intensity of the *i*th observation of reflection *hkl*. ⟨I(*hkl*)⟩is the mean value and the summation is over all measurements.
[c] $R_{work} = \sum_h\sum_i||F_o|-|F_c||/\sum|F_o|$.
[d] R_{free} is R_{work} for approximately 5% of the reflections that were excluded from the refinement.

3.2. Metal-binding sites

Similar to TcAE206 and CtCes3-1, a calcium ion that does not affect the enzymatic activity was observed the N-terminal end of the central β-strand (β2) in S10A (Fig. 1) [14,16]. Interestingly, significant electron density coordinated in a distorted octahedral form with six coordination bonds was also observed: Asp56 (OD1 and OD2), three water molecules, and His98 (NE2) in crystallographic symmetry. These features are not present in the structures of wild-type TcAE206, CtCes3-1, or Sm23 [14–16]. We assigned a zinc ion to this electron density based on electron density size, shape, and coordination number, which is appropriate based on the presence of $ZnSO_4$ in the crystallization solution. It is assumed that introduction of this zinc ion further strengthens the hydrogen bond network between neighboring molecules. Calcium and zinc ions are located sufficiently far from the active site that they are presumed to contribute to stabilization of the structure rather than catalytic activity.

3.3. Surface environment of the active site entrance

Although the key residues of the active site are completely conserved in TcAE206 and CtCes3-1, the substrate specificity of TcAE206 (S10A) differs from that of CtCes3-1 [14,16]. As mentioned in the "Introduction" section, Sm23 was omitted from this comparison because acetylated xylans (polysaccharides) and oligosaccharides were not used as substrates [15]. Nucleophilic Ser10 (substituted with Ala in this study) and additional residues that form the oxyanion hole (Gly62 and Asn92) are located in the small cavity, and the catalytic triad residues Asp179 and His182 are also located near this region (Fig. 2A). The cavity is approximately 6.0 × 7.0 × 6.0 Å (vertical × horizontal × depth) in TcAE206 (S10A) and 6.5 × 7.0 × 10 Å in CtCes3-1. Although the cavity in each enzyme has sufficient volume to accommodate an acetate group,

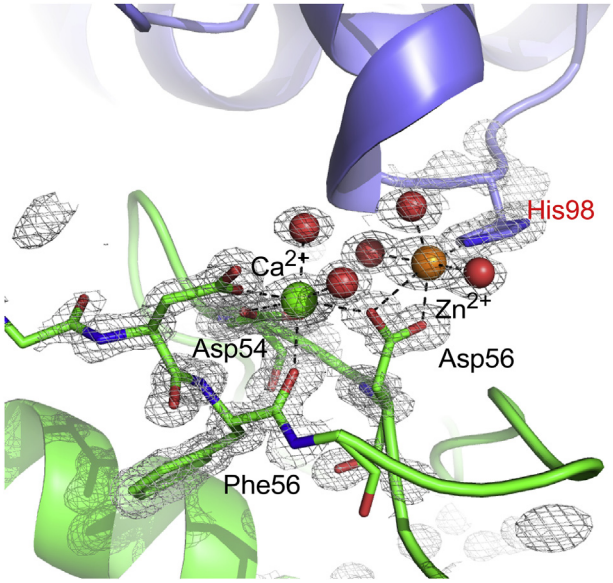

Fig. 1. Surface metal ion–binding site in S10A. 2*Fo*–*Fc* electron density map surrounding the metal ion–binding site in S10A are contoured at the 1.0-σ level in gray color. The residues of S10A are shown as a green-stick model, and oxygen and nitrogen atoms are shown in red and blue, respectively. Water molecules are illustrated as red-sphere models. Ca^{2+} and Zn^{2+} ions are shown as green- and orange-sphere models, respectively. His98 in the crystal symmetric subunit is shown in marine color and labeled in red. Hydrogen bonds are shown as dashed lines. (For interpretation of the references to colour in this figure legend, the reader is referred to the web version of this article.)

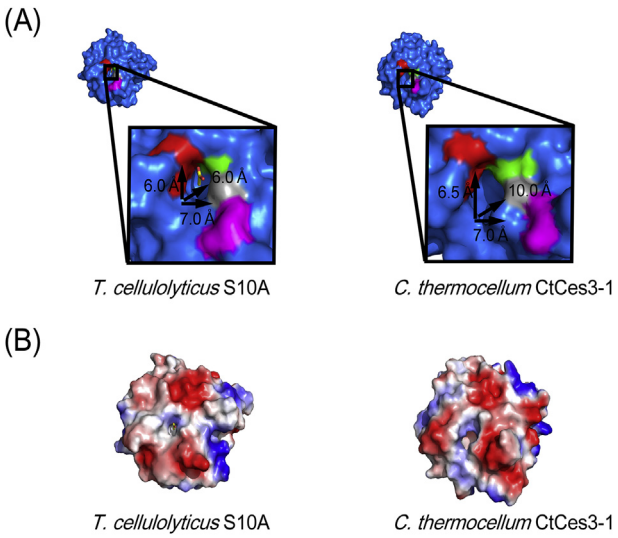

Fig. 2. Surface structure models of TcAE206_S10A and CtCes3-1. (A) Surface model of S10A and CtCes3-1 (sky-blue). The residues of the catalytic triad and oxyanion hole in S10A are shown as follows: Ser10Ala in green, Asp179 in magenta, His182 in gray, and Gly62 and Asn92 in red. The corresponding residues in CtCes3-1 are shown in the same colors. The acetate ion in S10A is shown as a yellow-stick model. (B) Electron potential maps of S10A and CtCes3-1. Positively and negatively charged regions are illustrated in red and blue, respectively. (For interpretation of the references to colour in this figure legend, the reader is referred to the web version of this article.)

the total cleft volume of S10A is substantially smaller than that of CtCes3-1: pocket volumes of approximately 140 $Å^3$ (S10A) and 250 $Å^3$ (CtCes3-1), respectively, as calculated using the CASTp server (http://cast.engr.uic.edu) [25]. Correia et al. reported that the internal cavity of CtCes3-1 may be able to accommodate more bulky polysaccharide substrates [14]. Our complex structure supports their conclusion because our data provide an explanation as to why TcAE206 does not exhibit enzyme activity toward polysaccharide substrates.

We also compared electron potential maps for the areas around the hydrophobic pockets of S10A and CtCes3-1 (Fig. 2B). S10A forms a flat surface around the pocket, whereas protrusions on both sides of the active site pocket are apparent with CtCes3-1. The area around the pocket region of S10A is more hydrophobic than the area around the pocket of CtCes3-1; S10A has few charged residues in this area to interact with a carbohydrate moiety. Therefore, in comparison with CtCes3-1, it appears to be less favorable for TcAE206 to bind long substrates (i.e., polysaccharides).

3.4. Active site structure of the TcAE206 mutant (S10A)

Prior to this study, in which we solved the structure of the mutant active site (TcAE206_S10A) complexed with an acetate ion (a product of D-glucose pentaacetate) (Fig. 3A), no substrate/product structure of a CE3 family enzyme had been reported. S10A assumes the SGNH-hydrolase superfamily structure; the key residues constituting the catalytic triad (Ser10Ala, Asp179, and His182) and oxyanion hole (Ser10Ala, Gly62, and Asn92) are completely conserved, as described above. Some SGNH-hydrolases, such as coronavirus hemagglutinin-esterase (PDB code 3cl5) [26], platelet-activating acetyl hydrolase (PDB code 1wab) [27], and *Neisseria meningitides* peptidoglycan *O*-acetylesterase (PDB code 4k7j) [28], reportedly form a complex with an acetate ion at a position equivalent to that in S10A. Therefore, the acetate ion in S10A is considered to be located in the correct position for catalytic activity [26–28]. The acetate ion (O) in S10A forms three hydrogen bonds:

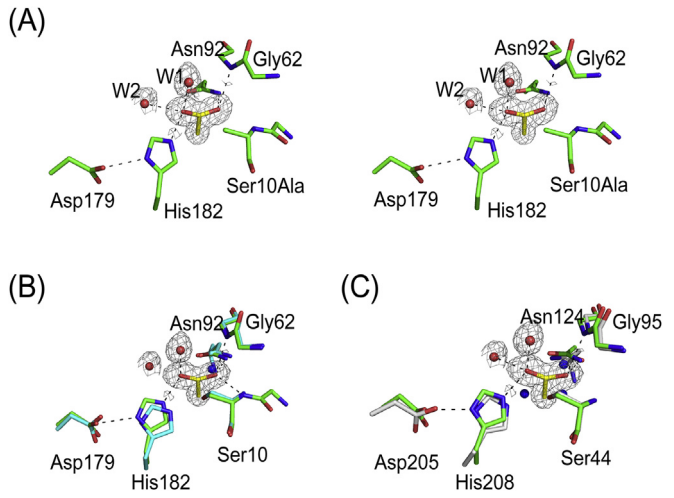

Fig. 3. Active site structure of CE3 acetyl esterases. (A) Stereo view of the active site of S10A (green-stick model) complexed with an acetate ion (yellow-stick model). Water molecules (W1 and W2; red spheres) were illustrated using the PyMol program. (B) TcAE206 (cyan-stick model) superimposed on the S10A structure. The water molecule in TcAE206 is shown as a blue-sphere model. (C) CtCes3-1 (gray-stick model) is superimposed on the S10A structure. The three water molecules in CtCes3-1 are shown as blue-sphere models. (For interpretation of the references to colour in this figure legend, the reader is referred to the web version of this article.)

with the side chain of Asn92 (ND), the main chain amide of Ala10, and Gly62, at distances of 2.8, 2.9, and 2.9 Å, respectively (Fig. 3A). These three hydrogen bonds have been observed in other SGNH-hydrolases as well [26–28]. The acetate ion is thought to stabilize the oxyanion hole by forming hydrogen bonds. Interestingly, the position of the acetate ion is normally occupied by a water molecule, essentially stabilizing the formation of the oxyanion hole in TcAE206 (Fig. 3B) and CtCes3-1 (Fig. 3C).

Moreover, the oxygen atom (OXT) of the acetate ion forms hydrogen bonds with the side chain of His182 (NE2) and two water molecules (W1 and W2), at distances of 2.5, 2.6, and 2.7 Å, respectively (Fig. 3A). Water molecules corresponding to W1 and W2 were not observed in TcAE206, however, both water molecules were far away from the generally basic residue His182 to play as the hydrolytic water; W1 and W2 were located 3.9 and 3.8 Å away from His182 (NE2), respectively.

Although the nucleophilic Ser was substituted with an Ala residue in TcAE206, the structures of the main chain and its neighboring residues were similar to those of TcAE206 (Fig. 3B). In contrast, the main chains of Gly62 and Asp179 and the side chain of Asn92 (ND) are slightly close to the acetate ion. In addition, His182 (NE2) moves 0.8 Å further toward the center of the active site (acetate ion) than does His182 (NE2) of TcAE206 (Fig. 3B). The His residue is thought to play a key role in the catalytic activity of serine esterases, as described below. In the absence of substrate, Ser10 forms a hydrogen bond with His182 (Fig. 4, step 1). In the presence of substrate, the nucleophilic Ser is deprotonated by the generally basic His residue in cooperation with the generally acidic Asp and then attacks the carbonyl carbon of the substrate (Fig. 4, step 2 and 3). The resulting tetrahedral intermediate rapidly breaks down to a covalent acyl-enzyme (Ser–acetyl group) and alcohol moiety (Fig. 4, step 4). By releasing the alcohol moiety, a space is made for the hydrolytic water molecule. The hydrolytic water molecule is also deprotonated by the His residue, and the resulting hydroxyl anion attacks the acyl-enzyme (Fig. 4, step 5 and 6), thereby returning the Ser residue to a protonated state so that it is ready for the next reaction (Fig. 4 step 1). Our data suggest that the His residue should move toward the center of the active site to facilitate these two deprotonation steps.

In conclusion, our complex structure does not provide sufficient detail to fully elucidate the interaction between the carbohydrate

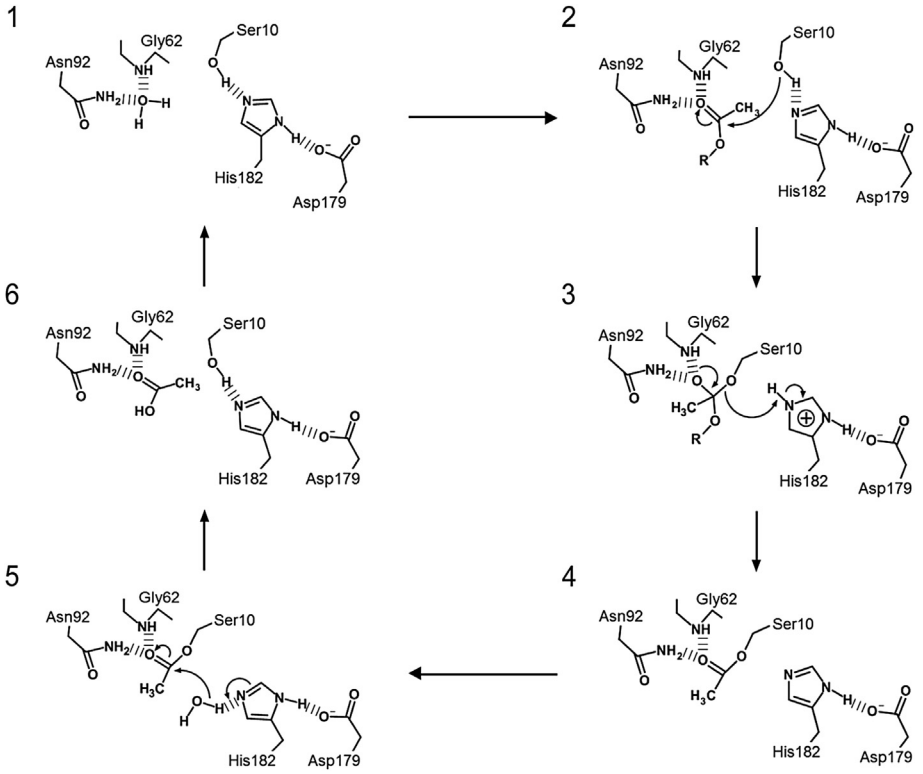

Fig. 4. Scheme of the catalytic reaction of fungal carbohydrate family 3 enzymes. R indicates the carbohydrate moiety of the substrate.

moieties and amino acids. Experiments designed to solve the complex structure of TcAE206 are currently ongoing, with the goal of elucidating the detailed catalytic mechanism of TcAE206 and the structural basis of its specificity for acetylated carbohydrate substrates.

PDB accession number

The coordinates and structural features of TcAE206_S10A complexed with an acetate ion were deposited in the Protein Data Bank under accession code 5B5L.

Conflict of interest

The authors declare no conflict of interest.

Acknowledgements

The X-ray diffraction data were obtained at the beamline BL44XU at SPring-8, Hyogo, Japan, with the approval of the Institute for Protein Research, Osaka University, Osaka, Japan (Proposal Nos. 2015A6559 and 2015B6559). The authors greatly thank Dr. Masaru Yoshida for his comments on the figures. This work was supported by the New Energy and Industrial Technology Development Organization (NEDO) (Grant Number 13401477-0).

Transparency document

Transparency document related to this article can be found online at http://dx.doi.org/10.1016/j.bbrc.2016.06.093.

Appendix A. Supplementary data

Supplementary data related to this article can be found at http://dx.doi.org/10.1016/j.bbrc.2016.06.093.

References

[1] R. Kumar, S. Singh, O.V. Singh, Bioconversion of lignocellulosic biomass: biochemical and molecular perspectives, J. Ind. Microbiol. Biotechnol. 35 (2008) 377–391.
[2] K. Keegstra, Plant cell walls, Plant Physiol. 154 (2010) 483–486.
[3] A. Sunna, G. Antranikian, Xylanolytic enzymes from fungi and bacteria, Crit. Rev. Biotechnol. 17 (1997) 39–67.
[4] R. Deutschmann, R.F.H. Dekker, From plant biomass to bio-based chemicals: latest developments in xylan research, Biotechnol. Adv. 30 (2012) 1627–1640.
[5] J. van den Brink, R.P. de Vries, Fungal enzyme sets for plant polysaccharide degradation, Appl. Microbiol. Biotechnol. 91 (2011) 1477–1492.
[6] L.P. Christov, B.A. Prior, Esterases of xylan-degrading microorganisms: production, properties, and significance, Enzyme Microb. Technol. 15 (1993) 460–475.
[7] P. Biely, Microbial carbohydrate esterases deacetylating plant polysaccharides, Biotechnol. Adv. 30 (2012) 1575–1588.
[8] L.M.A. Ferreira, T.M. Wood, G. Williamson, C. Faulds, G.P. Hazlewood, G.W. Black, H.J. Gilbert, A modular esterase from *Pseudomonas fluorescens* subsp. *cellulosa* contains a non-catalytic cellulose-binding domain, Biochem. J. 294 (1993) 349–355.
[9] V. Lombard, H.G. Ramulu, E. Drula, P.M. Coutinho, B. Henrissat, The carbohydrate-active enzymes database (CAZy) in 2013, Nucleic Acids Res. 42 (2014) D490–D495.
[10] J.M. Pfeffer, J.T. Weadge, A.J. Clarke, Mechanism of action of *Neisseria gonorrhoeae O*-acetylpeptidoglycan esterase, an SGNH serine esterase, J. Biol. Chem. 288 (2013) 2605–2613.
[11] E. Topakas, S. Kyriakopoulos, P. Biely, J. Hirsch, C. Vafiadi, P. Christakopoulos, Carbohydrate esterases of family 2 are 6-*O*-deacetylases, FEBS Lett. 584 (2010) 543–548.
[12] N. Hakulinen, M. Tenkanen, J. Rouvinen, Three-dimensional structure of the catalytic core of acetylxylan esterase from *Trichoderma reesei*: insights into the deacetylation Mechanism, J. Struct. Biol. 132 (2000) 180–190.
[13] D. Ghosh, M. Sawicki, P. Lala, M. Erman, W. Pangborn, J. Eyzaguirre, R. Gutiérrez, H. Jörnvall, D.J. Thiel, Multiple conformations of catalytic serine and histidine in acetylxylan esterase at 0.90 Å, J. Biol. Chem. 276 (2001) 11159–11166.
[14] M.A.S. Correia, J.A. Prates, J. Brás, C.M.G.A. Fontes, J.A. Newman, R.J. Lewis, H.J. Gilbert, J.E. Flint, Crystal structure of a cellulosomal family 3 carbohydrate esterase from *Clostridium thermocellum* provides insights into the mechanism of substrate recognition, J. Mol. Biol. 379 (2008) 64–72.
[15] K. Kim, B.H. Ryu, S.S. Kim, D.R. An, T.D. Ngo, R. Pandian, K.K. Kim, T.D. Kim, Structural and biochemical characterization of a carbohydrate acetylesterase from *Sinorhizobium meliloti* 1021, FEBS Lett. 589 (2015) 117–122.
[16] M. Watanabe, H. Fukada, H. Inoue, K. Ishikawa, Crystal structure of an acetylesterase from *Talaromyces cellulolyticus* and the importance of a disulfide bond near the active site, FEBS Lett. 589 (2015) 1200–1206.
[17] Z. Otwinowski, W. Minor, [20] Processing of X-ray diffraction data collected in oscillation mode, Methods Enzym. 276 (1997) 307–326.
[18] Collaborative Computational Project, Number 4, the CCP4 suite: programs for protein crystallography, Acta Crystallogr. Sect. D. Biol. Crystallogr. 50 (1994) 760–763.
[19] A.J. McCoy, R.W. Grosse-Kunstleve, P.D. Adams, M.D. Winn, L.C. Storoni, R.J. Read, Phaser crystallographic software, J. Appl. Crystallogr. 40 (2007) 658–674.
[20] P. Emsley, K. Cowtan, Coot: model-building tools for molecular graphics, Acta Crystallogr. Sect. D. Biol. Crystallogr. 60 (2004) 2126–2132.
[21] G.N. Murshudov, P. Skubák, A.A. Lebedev, N.S. Pannu, R.A. Steiner, R.A. Nicholls, M.D. Winn, F. Long, A.A. Vagin, REFMAC5 for the refinement of macromolecular crystal structures, Acta Crystallogr. Sect. D. Biol. Crystallogr. 67 (2011) 355–367.
[22] S.C. Lovell, I.W. Davis, W.B. Arendall 3rd, P.I.W. de Bakker, J.M. Word, M.G. Prisant, J.S. Richardson, D.C. Richardson, Structure validation by Cα geometry: Φ, Ψ and Cβ deviation, Proteins 50 (2003) 437–450.
[23] L.L.C. Schrödinger, The PyMOL Molecular Graphics Systems, 2015 version 1.7.6.0.
[24] B.W. Matthews, Solvent content of protein crystals, J. Mol. Biol. 33 (1968) 491–497.
[25] J. Dundas, Z. Ouyang, J. Tseng, A. Binkowski, Y. Turpaz, J. Liang, CASTp: computed atlas of surface topography of proteins with structural and topographical mapping of functionally annotated residues, Nucleic Acids Res. 34 (2006) W116–W118.
[26] Q. Zeng, M.A. Langereis, A.L.W. van Vliet, E.G. Huizinga, R.J. de Groot, Structure of coronavirus hemagglutinin-esterase offers insight into corona and influenza virus evolution, Proc. Natl. Acad. Sci. U. S. A. 105 (2008) 9065–9069.
[27] Y.S. Ho, L. Swenson, U. Derewenda, L. Serre, Y. Wei, Z. Dauter, M. Hattori, T. Adachi, J. Aoki, H. Arai, K. Inoue, Z.S. Derewenda, Brain acetylhydrolase that inactivates platelet-activating factor is a G-protein-like trimer, Nature 385 (1997) 89–93.
[28] A.H. Williams, F.J. Veyrier, M. Bonis, Y. Michaud, B. Raynal, M.K. Taha, S.W. White, A. Haouz, I.G. Boneca, Visualization of a substrate-induced productive conformation of the catalytic triad of the *Neisseria meningitidis* peptidoglycan *O*-acetylesterase reveals mechanistic conservation in SGNH esterase family members, Acta Crystallogr. Sect. D. Biol. Crystallogr. 70 (2014) 2631–2639.
[29] J.D. Thompson, D.G. Higgins, T.J. Gibson, CLUSTAL W: improving the sensitivity of progressive multiple sequence alignment through sequence weighting, position specific gap penalties and weight matrix choice, Nucleic Acids Res. 22 (1994) 4673–4680.
[30] P. Gouet, X. Robert, E. Courcelle, ESPript/ENDscript: extracting and rendering sequence and 3D information from atomic structures of proteins, Nucleic Acids Res. 31 (2003) 3320–3323.